OFFICE OF NAVAL RESEARCH

Contract N00014-89-J-1497

R&T Code 413050. . .02

Technical Report No. 29

Understanding Heterolytic Bond Cleavage

by

J. Simons and P. B. Armentrout

Prepared for Publication in

The Journal of the American Chemical Society

The University of Utah
Department of Chemistry
Salt Lake City, Utah 84112-1194

May 31, 1992

UNCLASSIFIED

SECURITY CLASSIFICATION OF THIS PAGE

REPORT DOCUMENTATION PAGE

1a. REPORT SECURITY CLASSIFICATION UNCLASSIFIED	1b RESTRICTIVE MARKINGS
2a. SECURITY CLASSIFICATION AUTHORITY	3 DISTRIBUTION / AVAILABILITY OF REPORT APPROVED FOR PUBLIC RELEASE: DISTRIBUTION UNLIMITED
2b. DECLASSIFICATION / DOWNGRADING SCHEDULE	
4. PERFORMING ORGANIZATION REPORT NUMBER(S) ONR TECHNICAL REPORT # 29	5. MONITORING ORGANIZATION REPORT NUMBER(S)
6a. NAME OF PERFORMING ORGANIZATION THE UNIVERSITY OF UTAH 6b OFFICE SYMBOL (If applicable)	7a. NAME OF MONITORING ORGANIZATION OFFICE OF NAVAL RESEARCH CHEMISTRY PROGRAM
6c. ADDRESS (City, State, and ZIP Code) DEPARTMENT OF CHEMISTRY UNIVERSITY OF UTAH SALT LAKE CITY, UT 84112	7b. ADDRESS (City, State, and ZIP Code) 800 NO. QUINCY ST. ARLINGTON, VA 22217-5000
8a. NAME OF FUNDING / SPONSORING ORGANIZATION OFFICE OF NAVAL RESEARCH 8b. OFFICE SYMBOL (If applicable) ONR	9. PROCUREMENT INSTRUMENT IDENTIFICATION NUMBER N00014-89-J-1497
8c. ADDRESS (City, State, and ZIP Code) 800 NO. QUINCY ST. ARLINGTON, VA 22217	10. SOURCE OF FUNDING NUMBERS PROGRAM ELEMENT NO. / PROJECT NO. / TASK NO. / WORK UNIT ACCESSION NO

11. TITLE (Include Security Classification)

"UNDERSTANDING HETEROLYTIC BOND CLEAVAGE"

12. PERSONAL AUTHOR(S)
P. B. Armentrout and Jack Simons

13a. TYPE OF REPORT	13b. TIME COVERED	14. DATE OF REPORT (Year, Month, Day)	15 PAGE COUNT
TECHNICAL	FROM 7/91-5/92 TO	5/31/92	

16. SUPPLEMENTARY NOTATION

SUBMITTED TO: The Journal of the American Chemical Society

17 COSATI CODES			18 SUBJECT TERMS (Continue on reverse if necessary and identify by block number)
FIELD	GROUP	SUB-GROUP	

19 ABSTRACT (Continue on reverse if necessary and identify by block number)

When considering the fragmentation of a single bond, the attractive singlet and repulsive triplet potential energy curves of the prototype H_2 - 2 H dissociation often come to mind. For species in which homolytic bond cleavage is energetically favored, such comparisons are reasonable. For other species where heterolytic cleavage gives lower-energy products, the H_2 analogy is inappropriate. This paper offers a qualitative theoretical treatment of the singlet and triplet potential energy curves that arise when a single bond formed by an electron pair is cleaved either homolytically or heterolytically. This analysis is shown to provide insght into several problems involving transition metal systems: transition metal carbonyls, metal ion-ligand complexes, and transition metal dimers.

20 DISTRIBUTION / AVAILABILITY OF ABSTRACT ☒ UNCLASSIFIED/UNLIMITED ☐ SAME AS RPT ☐ DTIC USERS	21 ABSTRACT SECURITY CLASSIFICATION UNCLASSIFIED
22a NAME OF RESPONSIBLE INDIVIDUAL PROFESSOR JACK SIMONS	22b TELEPHONE (Include Area Code) (801) 581-8023 / 22c. OFFICE SYMBOL

DD FORM 1473, 84 MAR 83 APR edition may be used until exhausted. All other editions are obsolete.

SECURITY CLASSIFICATION OF THIS PAGE

submitted to J. Am. Chem. Soc.

Understanding Heterolytic Bond Cleavage

P. B. Armentrout*,† and Jack Simons*

Chemistry Department

University of Utah

Salt Lake City, Utah 84112

Abstract

When considering the fragmentation of a single bond, the attractive singlet and repulsive triplet potential energy curves of the prototype $H_2 \rightarrow 2\ H$ dissociation often come to mind. For species in which homolytic bond cleavage is energetically favored, such comparisons are reasonable. For other species where heterolytic cleavage gives lower-energy products, the H_2 analogy is inappropriate. This paper offers a qualitative theoretical treatment of the singlet and triplet potential energy curves that arise when a single bond formed by an electron pair is cleaved either homolytically or heterolytically. This analysis is shown to provide insight into several problems involving transition metal systems: transition metal carbonyls, metal ion-ligand complexes, and transition metal dimers.

†Camille and Henry Dreyfus Teacher-Scholar, 1987-1992.

I. Introduction

As chemists, much of our intuition concerning chemical bonds is built on simple models introduced in undergraduate chemistry courses. The detailed examination of the H_2 molecule via the valence bond and molecular orbital approaches forms the basis of our thinking about bonding when confronted with new systems. Ordinarily, when we imagine bringing two radicals X• and Y• (each having a doublet spin state) together to form a single covalent bond, we anticipate that a bonding singlet state and a repulsive triplet state of the XY molecule are formed, much as they are for H_2. However, we have recently encountered several systems in which this picture of the bonding is incomplete and for which this simple intuition has led to flawed analyses involving qualitatively incorrect potential energy surfaces.

These cases involve species that dissociate heterolytically, i.e., during cleavage of a covalent bond one of the fragments retains both bonding electrons and these fragments have energies below those where each fragment retains a single electron. Far from being unusual, a preference for heterolytic bond cleavage arises quite naturally in systems involving transition metals, where interactions between empty metal orbitals and 2-electron donor ligands are ubiquitous. This situation is qualitatively different than in the case of H_2, where the $H^+ + H^-$ asymptote lies at much higher energies than H + H. The purpose of this paper is to outline how to correctly assess the qualitative characteristics of the potential energy surfaces involved in bonds that cleave heterolytically.

The theoretical methods and concepts included in this work are not new. Indeed, a series of articles by Poss and Shaik apply a valence-bond picture to explain the singlet-state potential energy surfaces that characterize a wide

variety of prototypical organic reactions, including cation-anion recombination,[1] donor-acceptor interactions,[2,3] elimination reactions,[4] and solution-phase S_N2 reactions.[5] This previous work demonstrates that the ideas discussed here have a very broad applicability. In the present paper, the roles of spin and permutational symmetry in determining which asymptotic states connect to which states of the XY molecule are treated in more detail than in references 1-5, and the results are directed at elucidating transition metal systems.

II. Summary of the State Correlations

To consider why the two-orbital two-electron single bond formation case can be more complex than often thought, consider the H_2 system in detail. In the molecular orbital (mo) description of H_2, both bonding σ_g and antibonding σ_u mos appear. There are two electrons that can both occupy the σ_g mo to yield the $^1\Sigma_g^+(\sigma_g^2)$ ground electronic state; however, they can also occupy both mos to yield $^3\Sigma_u^+(\sigma_g^1\sigma_u^1)$ and $^1\Sigma_u^+(\sigma_g^1\sigma_u^1)$, or both can occupy the σ_u mo to give the $^1\Sigma_g^+(\sigma_u^2)$ state. As demonstrated explicitly in Appendix A, the former two states dissociate homolytically to X• + X• = H + H, and the latter two dissociate heterolytically to X + X:$^-$ = H^+ + H^-. (In all cases considered here, only two electrons play active roles in the bond formation. The symbols X, X•, and X:$^-$ are used to denote species in which neither, one, or both bonding electrons, respectively, are attached to the X-fragment.) In the case of H_2 and for many other systems, the latter two states are sufficiently high in energy relative to the former two that they can be (and often are) ignored.

For several systems studied in our recent research, we have confronted situations where one of the heterolytic bond dissociation asymptotes (X + Y:$^-$

or $X^{:}$ + Y) is <u>lower</u> in energy than the homolytic bond dissociation asymptote. In such cases, σ bonding and σ^* antibonding mos are formed from the X and Y fragment orbitals. As in the H_2 case, occupying these two orbitals with two electrons gives rise to six electronic states: three singlets, $^1\Sigma(\sigma^2)$, $^1\Sigma^*(\sigma^1\sigma^{*1})$ and $^1\Sigma^{**}(\sigma^{*2})$, and a set of three degenerate triplets, $^3\Sigma^*(\sigma^1\sigma^{*1})$.

When heterolytic bond cleavage is favored, the states that are analogues of the $^1\Sigma_u^+(\sigma_g^1\sigma_u^1)$ and $^1\Sigma_g^+(\sigma_u^2)$ states of H_2 (the $^1\Sigma^*$ and $^1\Sigma^{**}$ states) cannot be ignored in understanding the valence states of the XY molecules. The presence and character of these states are <u>essential</u> to a proper treatment of cases in which heterolytic bond cleavage is favored. Details necessary for understanding the relative energies of all six electronic states and to which separated asymptote they dissociate are outlined in Appendix A. For the homonuclear case, descriptions of the valence singlet and triplet Σ states are given in Figs. 1 and 2 for situations in which covalent products lie below and above ionic products, respectively. The extensions of these state correlation diagrams to the heteronuclear situations are described in Figs. 3 (when homolytic cleavage is favored), 4 (when $X^{:}$ + Y is below X• + Y• which lies below X + $Y^{:}$), and 5 (when $X^{:}$ + Y and X + $Y^{:}$ both lie below X• + Y•). A key feature in all five of these figures is that there is one and only one singlet surface that is an attractive (bonding) potential energy curve. The two other singlet surfaces are repulsive, as are the three triplet surfaces. The variations among the figures are due to mixing of the $^1\Sigma$, $^1\Sigma^*$, and $^1\Sigma^{**}$ configurations (in the homonuclear cases, only the $^1\Sigma$ and $^1\Sigma^{**}$ configurations mix since these have gerade symmetry while $^1\Sigma^*$ has ungerade symmetry), which varies with bond distance. As the energy ordering of the asymptotes varies from Fig. 1 to 2 and from Fig. 3 to 5, so do these correlations and so does

the molecular state that connects to each asymptote.

The characterization of repulsive surfaces in Figs. 1 - 5 is based only on contributions to the inter-fragment interactions that arise from valence-orbital couplings. If one or both of the X and Y fragments possess a net charge, the qualitative potential surfaces described here are modified by any coulombic, charge-dipole, or charge-induced-dipole energies. Such additional factors can lead to attractive long-range interactions typical of ion-molecule complexes, and thereby modify the strictly repulsive character of the excited state surfaces shown in Figs. 1 - 5.

III. Application to Experimentally Studied Species

A. Photodissociation of Silicon-Silicon Bonds. As we were writing this paper, Michl published a short pedagogical paper[6] based on ideas similar to those discussed here. His contribution focuses on why carbon-carbon bonds have a much larger <u>singlet</u> $\sigma \rightarrow \sigma^*$ excitation energy than silicon-silicon bonds. In our terminology, such an excitation corresponds to a transition from the $^1\Sigma_g^+$ surface to the $^1\Sigma_u^{+*}$ surface of Fig. 1; this is a case in which the homolytic cleavage products lie lower in energy. The Michl article points out that this excitation energy is largely determined by the spacing between the homolytic and heterolytic asymptotes, which, in turn, is determined by the ionization energy minus electron affinity of the X• and Y• radicals involved. Since the ionization energy of R_3Si species is smaller than that of R_3C radicals and the electron affinity of R_3Si is greater than that of R_3C, the gap between the homolytic and heterolytic dissociation asymptotes for silicon-silicon bonded species is smaller than for carbon-based fragments.

B. Transition Metal Carbonyls. One class of intensely studied

molecules where heterolytic bond cleavage is taken for granted is the transition metal carbonyls, $M(CO)_{x+1}$. Carbonyls are the quintessential two-electron donor ligand and thus dissociation of a metal carbonyl complex along its ground electronic surface will involve heterolytic bond cleavage to form $M(CO)_x + CO = Y + X:$. This is shown in the qualitative schematic potential energy surface of Fig. 6, taken from a recent study of manganese carbonyl cations by Dearden *et al.*[7] Here, the $Mn(CO)_{x+1}^+$ species (in either its ground or excited state) dissociates to form $Mn(CO)_x^+ + CO$. Unfortunately, Fig. 6 contains a fundamental mistake, namely there can be no repulsive surface evolving from the dissociation asymptotes shown.

This can be seen by ascertaining the species involved in the other dissociation asymptotes. Homolytic cleavage of the Mn-CO bond corresponds to formation of $Mn(CO)_x + CO^+$ and is much higher in energy than the $Mn(CO)_x^+ + CO$ asymptote since the ionization energy of the metal containing fragment is much lower than that of CO. The other heterolytic asymptote, $Y: + X$, corresponds to generation of $Mn(CO)_x^- + CO^{2+}$, and is even higher in energy. Thus, Fig. 4 is the appropriate diagram for this system, as well as for all neutral, cationic and anionic metal carbonyls. (In neutral and anionic systems, homolytic cleavage corresponds to the high energy products $M(CO)_x^- + CO^+$ and $M(CO)_x^{2-} + CO^+$, respectively.)

The experimental work of Dearden et al. was designed to investigate how the spin state of the metal carbonyl might change with the number of ligands and how spin conservation might influence the bonding energetics and dissociation characteristics of these molecules. They considered that the repulsive curve shown in Fig. 6 might be the result of a spin-forbidden dissociation process and the crossing between the repulsive surface and the

excited state attractive surface could therefore lead to a barrier to dissociation. The results of Fig. 4 show that no repulsive surface can evolve from either $Mn(CO)_x^+$ + CO asymptote, regardless of the spin of these species.

Experimentally, Dearden et al. found that there are no barriers for addition of CO to $Mn(CO)_x^+$ (x = 1 - 5). This conclusion is, of course, not surprising given Fig. 4, which provides a proper qualitative characterization of the potential energy curves. Our work here reinforces the conclusion of Dearden *et al.* that if interactions between surfaces of different spin are occurring, they must be between attractive surfaces. This is consistent with our own discussion of dissociation in the $Fe(CO)_x^+$ (x = 1 - 5) system.[8]

C. **Silver-Benzene Cation.** Another system where the analysis discussed above can be used to understand recent experimental data is the silver-benzene ion, $(AgC_6H_6)^+$. Experiments by Willey et al.[9] find that this complex photodissociates exclusively to Ag + $C_6H_6^+$ when irradiated with laser light over a photon range of 386-266 nm (3.21 - 4.66 eV). This observation is intriguing because the lowest energy asymptote for dissociation is Ag^+ + C_6H_6 since the ionization energy of Ag (7.58 eV) is 1.66 eV below that of benzene (9.24 eV).[10] Willey et al. interpreted their results by using the schematic potential energy surfaces shown in Fig. 7.[11]

Consideration of the states of the dissociated fragments in this system suggest that $Ag^+(^1S,\ 5s^04d^{10})$ + $C_6H_6(X^1A_{1g})$ can be viewed as products of a heterolytic cleavage process in which benzene retains the pair of electrons used to form a bond in the complex. The $Ag(^2S,\ 5s^14d^{10})$ + $C_6H_6^+(X^2E_{1g})$ asymptote corresponds to homolytic cleavage of this bond. The alternate heterolytic cleavage generates $Ag^-(^1S,\ 5s^24d^{10})$ + $C_6H_6^{+2}$, which lies much higher in energy. While the details of the bonding in $(AgC_6H_6)^+$ are not addressed by

the simple two electron model discussed above, the qualitative aspects of the potential energy surfaces of this system should correspond to those shown in Fig. 4. Note that this figure differs from that of Willey et al. in that the upper surface does not have a significant bonding well. In truth, the upper surface in Fig. 4 is also not completely accurate since it does not account for the fact that this is an ion-molecule system. In particular, the repulsive curves should probably have weakly attractive components at long-range, but the overall character of the upper surface as repulsive in the region accessible by vertical transitions should largely be retained.

Given this diagram, the photophysics of this system become straightforward to understand. Excitation from the $^1\Sigma$-like ground-state surface of $(AgC_6H_6)^+$ (which dissociates to ground state $Ag^+ + C_6H_6$) to the $^1\Sigma^*$-like surface (which dissociates to $Ag + C_6H_6^+$) should be a strongly allowed transition since it has ($\sigma \rightarrow \sigma^*$) character. Moreover, the fact that the upper state is largely repulsive explains why dissociation to the excited state asymptote is so prevalent; as soon as the excited state is formed, the species dissociates with little probability of returning to the ground-state surface. The ion-induced dipole attractive component of the excited-state surface may provide an explanation for why photodissociation is observed at the thermodynamic limit (i.e., the $^1\Sigma^*$ curve may not be repulsive at long range).

D. Diatomic Transition Metal Cations. The necessity of understanding heterolytic bond cleavage first became evident to us in interpreting the dissociation of diatomic transition metal ions.[12,13,14] Most transition metal atoms have ground states with electron configurations of the form s^2d^n (for first-row metals, exceptions include $Cr(s^1d^5)$, $Cu(s^1d^{10})$, and the s^1d^9 state of Ni is nearly isoenergetic with the s^2d^8 ground state). The

corresponding positive ions have ground states with s^1d^n (Sc, Ti, Mn, Fe) or s^0d^{n+1} (V, Cr, Co, Ni, Cu) electron configurations. For each of these elements, the alternate electron configuration leads to low-lying excited states of the ion.

We can imagine forming an M_2^+ metal dimer ion with a configuration described as $\sigma_g^2d^nd^{n+1}$, where the σ_g bonding orbital is formed primarily from the metal s orbitals and the d orbitals are largely nonbonding[15] (as is particularly appropriate towards the right hand side of the periodic table). If the σ bond is homolytically broken, one forms $X\bullet + Y\bullet = M(s^1d^{n+1}) + M^+(s^1d^n)$. However, for most metals, this dissociation asymptote lies higher in energy than the heterolytic products, $X\!:^- + Y = M(s^2d^n) + M^+(s^0d^{n+1})$.

Iron dimer neutral and cation bond energies. Such considerations have been useful in understanding differences in the bonding energetics between neutral and cationic metal dimer ions. This is illustrated by Fe_2^+, also a case where confusion regarding the character of the dissociation asymptotes exists in the literature. The bond energies of Fe_2 and Fe_2^+ are 1.15 ± 0.09 and 2.72 ± 0.07 eV, respectively.[12] Rohlfing et al.[16] rationalized the weak neutral bond energy by noting that two Fe atoms in their $^5D(s^2d^6)$ ground state cannot form a strong bond. Rather, ground state $Fe_2(\sigma_g^2d^7d^7)$ correlates with association of two iron atoms in their $^5F(s^1d^7)$ state, 0.86 eV higher in energy than the atomic ground state.[17] (Note that heterolytic bond cleavage is unimportant here since this corresponds to $Fe^+ + Fe^-$, much higher in energy.) In essence, formation of ground state Fe_2 requires a promotion energy of 1.72 eV, such that the dissociation energy of the σ_g^2 bond is 2.87 eV relative to the 2 Fe(^5F, s^1d^7) asymptote.

In discussing the relatively higher bond energy for the Fe_2^+ dimer ion,

Morse commented that the promotion energy for this charge state was only 0.86 eV since ground state $Fe^+(^6D)$ already has a s^1d^6 configuration.[15] The implicit assumption here is that ground state $Fe_2^+(\sigma_g^2d^6d^7)$ dissociates homolytically to $Fe(s^1d^7) + Fe^+(s^1d^6)$, 0.86 eV above the $Fe(s^2d^6) + Fe^+(s^1d^6)$ ground state asymptote. As we have pointed out elsewhere,[12] heterolytic cleavage of this ground state dimer ion should actually form $Fe(s^2d^6) + Fe^+(s^0d^7)$, lying only 0.23 eV above the ground state asymptote. Relative to this asymptote, the dissociation energy of the σ_g^2 bond of Fe_2^+ is 2.95 eV, very similar to the value for the Fe_2 neutral. Thus, these promotion energy arguments quantitatively account for the large difference in the cationic and neutral dimer bond energies when the correct dissociation asymptotes are considered.

Complications. The details of the surfaces for Fe_2^+ and other transition metal dimer ions will, of course, be complicated by other considerations. When using the analysis discussed earlier (and treated in Appendix A) for homonuclear species that contain two electrons in two s-based orbitals and open d-shells, it is necessary to also consider the spin coupling and g and u symmetries of the states arising from the underlying d-based orbitals. As shown in Appendix B, for systems arising from atomic asymptotes of the form $s^2d^n + s^0d^{n+1}$, $s^1d^n + s^1d^{n+1}$, and $s^0d^n + s^2d^{n+1}$ (note that the latter asymptote corresponds to $M^{2+} + M^-$), it is possible to use our earlier analysis with the d^n "core" electrons treated as X and the d^{n+1} core viewed as Y. As a result, the potential curves such as depicted in Fig. 4 are expected when the $s^2d^n + s^0d^{n+1}$ asymptote is the lowest; Fig. 3 is expected if the $s^1d^n + s^1d^{n+1}$ species lie lowest. Likewise, Fig. 1 applies when dealing with neutral homonuclear transition metal dimers where the homolytic asymptote of $s^1d^n + s^1d^n$ configuration is lowest in energy.

Of course, this treatment assumes that the dominant part of the bonding and antibonding interactions arises from the s-based orbitals, and that the $d^n d^{n+1}$ cores play no role except in determining the relative ordering of the $s^2d^n + s^0d^{n+1}$, $s^1d^n + s^1d^{n+1}$, and $s^0d^n + s^2d^{n+1}$ asymptotes. This is most likely to be the case for late transition metal species for which the d orbitals are radially separated from the s orbitals. In reality, interactions between the open d shells on the atoms will give rise to families of potential surfaces that produce bands of states in place of the curves described here, although the qualitative behavior of these families of surfaces will be determined largely by the considerations outlined here.

Extension to cases involving one and three σ electrons. For real transition metal dimers, surfaces involving two electrons in a σ orbital will not fully represent the complexities since there will be additional surfaces corresponding to one or three σ electrons. These will evolve from asymptotes corresponding to $s^1d^{n+1} + s^0d^{n+1}$ and $s^2d^n + s^1d^n$, respectively. In both cases and in the absence of d interactions, one attractive curve (corresponding to $\sigma_g{}^1d^{n+1}d^{n+1}$ and $\sigma_g{}^2\sigma_u{}^{*1}d^nd^n$ occupancies, respectively) and one repulsive curve (of $\sigma_u{}^{*1}d^{n+1}d^{n+1}$ and $\sigma_g{}^1\sigma_u{}^{*2}d^nd^n$ occupancies, respectively) are expected from each asymptote. An example of the multitude of potential curves that can arise when one, two and three σ electrons are simultaneously present is shown in Fig. 8 for the case of Ni_2^+, which is discussed in more detail in the following section.

This simple picture is modified when the asymptotic $s^1d^{n+1} + s^0d^{n+1}$ (or $s^1d^n + s^2d^n$) states are split into high- and low-spin coupled states, as they are for the Ni_2^+ case (^3D vs ^1D states of Ni). Analogous considerations to those in the previous section can be used to analyze this situation. Here,

the high-spin asymptotic states produce two sets of $\sigma^1d^{n+1}d^{n+1}$ (or $\sigma^2\sigma^{*1}d^nd^n$) attractive curves and a set of $\sigma^{*1}d^{n+1}d^{n+1}$ (or $\sigma^1\sigma^{*2}d^nd^n$) repulsive curves. The higher energy low-spin asymptotic states produce another set of $\sigma^{*1}d^{n+1}d^{n+1}$ (or $\sigma^1\sigma^{*2}d^nd^n$) repulsive curves. Using the Ni + Ni^+ system as an example, the $Ni(^3D,s^1d^9)$ + $Ni^+(^2D,s^0d^9)$ asymptote produces a set of 100 bonding quartet $\sigma^1d^9d^9$ states, a set of 100 antibonding quartet $\sigma^{*1}d^9d^9$ states, and a set of 100 bonding doublet $\sigma^1d^9d^9$ states. The $Ni(^1D,s^1d^9)$ + $Ni^+(^2D,s^0d^9)$ asymptote produces a set of 100 antibonding doublet $\sigma^{*1}d^9d^9$ states and no bonding states. This pattern of potential energy curves is shown in Fig. 8. A similar pattern would appear for the molecular states with three σ electrons, e.g. $Ni(^3F,s^2d^8)$ + $Ni^+(^4F,s^1d^8)$ vs $Ni(^3F,s^2d^8)$ + $Ni^+(^2F,s^1d^8)$ asymptotes in the Ni_2^+ case. This latter asymptote is not shown since it is higher in energy than those included in Fig. 8.

Photodissociation of Ni_2^+. A case where this analysis allows the interpretation of recent experimental results is in the photodissociation of Ni_2Ar^+ as studied by Lessen and Brucat.[18] They found that this species dissociates primarily to Ni^+ at a photon energy of 3.49 eV, and to Ni_2^+ at 2.98 eV (some Ni^+ was observed at this photon energy but the signal was attributed to two-photon events). Thus, they assigned the bond energy of Ni_2^+ as 3.0 - 3.5 eV. In contrast, collision-induced dissociation studies conducted in one of our laboratories found a bond energy for Ni_2^+ of 2.08 ± 0.07 eV,[14] which is in agreement with recent ab initio calculations of Bauschlicher et al.[19]

This discrepancy can be understood by considering that Ni_2^+ has a ground state $\sigma_g^2d^8d^9$ configuration, as calculated by Bauschlicher et al.[19] and by Upton and Goddard.[20] This molecular state can dissociate heterolytically to

form ground state $Ni(s^2d^8)$ + $Ni^+(s^0d^9)$, while homolytic dissociation forms $Ni(s^1d^9)$ + $Ni^+(s^1d^8)$, 1.07 eV higher in energy.[17] The surfaces for Ni_2^+ are approximately as shown in Fig. 8, which also shows all other low energy asymptotes and the likely molecular states, including those obtained by more extensive calculations.[19,20] Transitions from the $Ni_2^+(\sigma_g^2d^8d^9)$ ($^1\Sigma$-like) ground state to the $Ni_2^+(\sigma_g^1\sigma_u^{*1}d^8d^9)$ ($^1\Sigma^*$-like) state correlating with homolytic dissociation should be strongly allowed and will lead to prompt dissociation to form Ni^+. Further, it seems likely that optical transitions at lower energies will not be strongly allowed since lower-lying molecular states correspond to s-d transitions, parity forbidden in the atom.

Therefore, we postulate that irradiation of Ni_2Ar^+ at 3.49 eV accesses this strong, dissociative transition. At a photon energy of 2.98 eV, no strongly repulsive states are easily formed and the Ni_2Ar^+ molecule dissociates primarily by Ar loss, and the Ni_2^+ species thus formed does not couple strongly to predissociative states and thus has a long lifetime. Note that the 1.07 eV excitation energy to the homolytic dissociation asymptote is sufficient to quantitatively account for the difference between the bond energy of Ni_2^+ as measured by collision-induced dissociation vs that from the photodissociation study.

Heteronuclear transition metal dimer ions. It should be noted that qualitative aspects of the above analysis for homonuclear transition metal dimer ions will persist for heteronuclear ions. For example, the ground-state dissociation asymptote for $CoNi^+$ is the heterolytic cleavage products $Co(s^2d^7)$ + $Ni^+(s^0d^9)$. The alternative heterolytic cleavage to form $Co^+(s^0d^8)$ + $Ni(s^2d^8)$ is 0.23 eV higher in energy. Both of the surfaces evolving from these asymptotes will be strongly attractive since they correspond to <u>different</u> d

orbital configurations on the two different nuclei, $\sigma^2d^7d^9$ and $\sigma^2d^8d^8$, respectively.[21] In contrast, homolytic cleavage leads to $Co^+(s^1d^7)$ + $Ni(s^1d^9)$, 0.45 eV above the ground state asymptote, and $Co(s^1d^8)$ + $Ni^+(s^1d^8)$, 1.47 eV higher.[17] These asymptotes lead to both high- and low-spin repulsive surfaces. Overall, for a given $d_X^n d_Y^n$ core configuration, the surfaces will correspond to those shown in Fig. 4.

The extent of this behavior can be seen by considering the 36 heteronuclear diatomic ions that can be formed from the first-row transition elements Sc-Cu. As throughout this paper, considering only species involving a single two-electron bond, one finds that 22 of 36 heteronuclear diatomic ions cleave heterolytically and 14 cleave homolytically.

IV. Summary

When interpreting results of dynamic and spectroscopic experiments involving dissociative species, it is essential to know how the electronic states accessed in the experiment correlate to states of the fragment species. Since state-of-the-art quantum chemistry calculations cannot be performed routinely on all possible systems of interest, there is a need for qualitative means of describing the relevant low-energy potential energy surfaces. When dealing with homolytic bond rupture, this is often achieved by analogy with the potential curves of the H_2 molecule. Unfortunately, species containing transition metals often dissociate heterolytically, so the H_2 paradigm is inappropriate. We believe that the work described here provides a general framework for understanding many interesting bond-breaking problems, including those in which heterolytic bond rupture is favored. By applying our analysis to several systems of immediate experimental interest, and by pointing out

qualitative errors in published potential energy surfaces, we attempt to illustrate the importance and utility of this framework.

APPENDIX A. Analysis of Two-Electron, Two-Orbital, Single-Bond Formation

A. Orbitals, Configurations and States. The six electronic states involved in two-orbital, two-electron systems can be described in terms of the six configuration state functions[22] (CSFs) that arise when one occupies the pair of bonding σ and antibonding σ^* molecular orbitals with two electrons. The CSFs are combinations of Slater determinants formed to generate proper spin- and spatial symmetry-functions. The essential features of all Slater determinant wavefunctions are: (i) that they each involve a product of N spin-orbitals and thus form an N-electron function, (ii) that they embody permutational antisymmetry of the wavefunction, (iii) and that they are normalized functions of the coordinates of the N electrons.

To describe the singlet CSF corresponding to the closed-shell σ^2 orbital occupancy, a single Slater determinant

$$^1\Sigma(0) = |\sigma\alpha\ \sigma\beta| = (2)^{-1/2}\ [\ \sigma\alpha(1)\ \sigma\beta(2) - \sigma\beta(1)\ \sigma\alpha(2)\ ]$$

suffices. An analogous expression for the $(\sigma^*)^2$ CSF is given by

$$^1\Sigma^{**}(0) = |\sigma^*\alpha\ \sigma^*\beta| = (2)^{-1/2}\ [\ \sigma^*\alpha(1)\ \sigma^*\beta(2) - \sigma^*\beta(1)\ \sigma^*\alpha(2)\ ].$$

Also, the $M_S = \pm 1$ components of the triplet state having $\sigma^1\sigma^{*1}$ orbital occupancy can be written as single Slater determinants:

$$^3\Sigma^*(1) = |\sigma\alpha\ \sigma^*\alpha| = (2)^{-1/2}\ [\ \sigma\alpha(1)\ \sigma^*\alpha(2) - \sigma^*\alpha(1)\ \sigma\alpha(2)\ ],$$

$$^3\Sigma^*(-1) = |\sigma\beta\ \sigma^*\beta| = (2)^{-1/2}\ [\ \sigma\beta(1)\ \sigma^*\beta(2) - \sigma^*\beta(1)\ \sigma\beta(2)\ ].$$

However, to describe the singlet CSF and $M_S = 0$ triplet CSF belonging to the $\sigma^1\sigma^{*1}$ occupancy, two Slater determinants are needed:

$$^1\Sigma^*(0) = 2^{-1/2}\ [\,|\sigma\alpha\ \sigma^*\beta| - |\sigma\beta\ \sigma^*\alpha|\,]$$

is the singlet CSF and

$$^3\Sigma^*(0) = 2^{-1/2} \left[|\sigma\alpha\ \sigma^*\beta| + |\sigma\beta\ \sigma^*\alpha| \right]$$

is the triplet CSF. In each case, the spin quantum number S, its z-axis projection M_S , and the Λ quantum number are given in the conventional $^{2S+1}\Lambda(M_S)$ notation.

B. Orbital Correlations. The σ and σ^* molecular orbitals (mos) are formed from orbitals of the constituent atoms or functional groups (denoted s_X and s_Y). The energy variation in these orbital energies with X-Y separation gives rise to variations in the energies of the six electronic states that arise as combinations of the above CSFs. For the homonuclear case, as R approaches ∞, the energies of the $\sigma = \sigma_g$ and $\sigma^* = \sigma_u$ orbitals become degenerate. In the heteronuclear case, the energy of the σ orbital approaches the energy of the lower s_X orbital, and the σ^* orbital converges to the higher s_Y orbital energy. Unlike the homonuclear case, the σ and σ^* orbitals are <u>not</u> degenerate as $R \rightarrow \infty$. The energy "gap" between the σ and σ^* orbitals at $R = \infty$ depends on the electronegativity difference between the groups X and Y. If this gap is small, it is expected that the behavior of this (slightly) heteronuclear system should approach that of the homonuclear X_2 and Y_2 systems.

C. State Correlation Diagrams. The three singlet, $^1\Sigma(0)$, $^1\Sigma^*(0)$, and $^1\Sigma^{**}(0)$, and three triplet, $^3\Sigma^*(1)$, $^3\Sigma^*(0)$ and $^3\Sigma^*(-1)$, CSFs are not the true electronic eigenstates of the system. Rather, the set of CSFs Φ_I of the same symmetry must be combined[22] to form the proper electronic eigenstates Ψ_K of the system:

$$\Psi_K = \sum_I C_I^K \Phi_I .$$

Within the approximation that the valence electronic states can be described

adequately as combinations of the above valence CSFs, the three $^1\Sigma$, $^1\Sigma^*$, and $^1\Sigma^{**}$ CSFs must be combined to form the three lowest energy valence electronic states of $^1\Sigma$ symmetry. In the heteronuclear case, all three singlet CSFs mix, while in the homonuclear case, the $^1\Sigma^*$ CSF, which has ungerade symmetry, does not couple with the $^1\Sigma$ and $^1\Sigma^{**}$ CSFs, which have gerade symmetry.

To understand the extent to which the $^1\Sigma$ and $^1\Sigma^{**}$ (and $^1\Sigma^*$ for heteronuclear cases) CSFs couple, it is useful to examine the energies of these CSFs for the range of internuclear distances of interest $R_e < R < \infty$. Near R_e, where the energy of the σ orbital is substantially below that of the σ^* orbital, the σ^2 ($^1\Sigma$) CSF lies significantly below the $\sigma^1\sigma^{*1}$ ($^1\Sigma^*$) CSF which, in turn lies below the σ^{*2} ($^1\Sigma^{**}$) CSF, the large energy splittings among these three CSFs simply reflecting the large gap between the σ and σ^* orbitals. The $^3\Sigma^*$ CSF generally lies below the corresponding $^1\Sigma^*$ CSF by an amount related to the exchange energy between the σ and σ^* orbitals.

As $R \rightarrow \infty$, the CSF energies are more difficult to "intuit" because the σ and σ^* orbitals become degenerate (in the homonuclear case) or nearly so (in the heteronuclear case). To pursue this point and arrive at an energy ordering for the CSFs appropriate to the $R \rightarrow \infty$ region, it is useful to express each of the above CSFs in terms of the fragments' active orbitals s_X and s_Y that comprise σ and σ^*. To do so, the LCAO-MO expressions for σ and σ^*,

$$\sigma = C\,[s_X + z\,s_Y] \quad \text{and} \quad \sigma^* = C^*\,[z\,s_X - s_Y],$$

are substituted into the Slater determinant definitions of the CSFs. Here C and C^* are normalization constants. The parameter z is 1.0 in the homonuclear case and deviates from 1.0 in relation to the s_X and s_Y orbital energy difference (if s_X lies below s_Y, then $z < 1.0$; if s_X lies above s_Y, $z > 1.0$).

A decomposition of the six CSFs listed in section A, using the molecular

orbitals introduced here yields:

$$^1\Sigma(0) = C^2 [|s_X\alpha\ s_X\beta| + z^2 |s_Y\alpha\ s_Y\beta| + z |s_X\alpha\ s_Y\beta| + z |s_Y\alpha\ s_X\beta|]$$

$$^1\Sigma^{**}(0) = C^{*2}[z^2 |s_X\alpha\ s_X\beta| + |s_Y\alpha\ s_Y\beta| - z |s_X\alpha\ s_Y\beta| - z |s_Y\alpha\ s_X\beta|]$$

$$^1\Sigma^{*}(0) = CC^* (2)^{-1/2} [2z |s_X\alpha\ s_X\beta| - 2z |s_Y\alpha\ s_Y\beta| + (z^2 - 1) |s_Y\alpha\ s_X\beta| + (z^2 - 1) |s_X\alpha\ s_Y\beta|]$$

$$^3\Sigma^{*}(0) = CC^* (2)^{-1/2} (z^2 + 1) [|s_Y\alpha\ s_X\beta| - |s_X\alpha\ s_Y\beta|]$$

$$^3\Sigma^{*}(1) = CC^* (z^2 + 1) |s_Y\alpha\ s_X\alpha|$$

$$^3\Sigma^{*}(-1) = CC^* (z^2 + 1) |s_Y\beta\ s_X\beta|.$$

Clearly, the three $^3\Sigma^*$ CSFs retain purely covalent character as $R \rightarrow \infty$ because each determinant describes an X• + Y• electron distribution. In this large-R limit, $^1\Sigma$, $^1\Sigma^{**}$, and $^1\Sigma^*$ CSFs possess covalent, $|s_X\alpha\ s_Y\beta| + |s_Y\alpha\ s_X\beta|$, and ionic, $|s_X\alpha\ s_X\beta|$ and $|s_Y\alpha\ s_Y\beta|$, components. (In the homonuclear limit, the $^1\Sigma^*$ CSF is purely ionic.) These singlet CSFs combine to produce the three true singlet states Ψ_K, one of which is a covalent function, $|s_X\alpha\ s_Y\beta| + |s_Y\alpha\ s_X\beta|$, of X• + Y• character, and two ionic wavefunctions, $|s_Y\alpha\ s_Y\beta|$ and $|s_X\alpha\ s_X\beta|$, having X + Y:⁻ and X:⁻ + Y character, respectively. At other values of R, these three CSFs will mix (in various amounts) to produce three energetically distinct singlet state surfaces. Plots of these energies vs R are called state correlation diagrams, and are shown in Fig. 3 for the case where E(X•) + E(Y•) < E(X:⁻) + E(Y) < E(X) + E(Y:⁻), Fig. 4 for E(X:⁻) + E(Y) < E(X•) + E(Y•) < E(X) + E(Y:⁻), and Fig. 5 for E(X:⁻) + E(Y) < E(X) + E(Y:⁻) < E(X•) + E(Y•).

APPENDIX B. Symmetry Analysis for Homonuclear Species Containing $d^n d^{n+1}$ Cores and Two Electrons in s-based Orbitals

The developments presented in Appendix A need to be extended somewhat to

cover homonuclear cases in which open-shell d orbitals are also present. For homonuclear ionic (cation or anion) species, dissociation must lead to fragments that contain different numbers of electrons. Given two electrons in the s-based orbitals, one can have $s^2d^n + s^0d^{n+1}$, $s^1d^n + s^1d^{n+1}$, or $s^0d^n + s^2d^{n+1}$ orbital occupancies on the fragments. For example, when Fe_2^+ dissociates, one can form the low-energy $Fe(s^2d^6) + Fe^+(s^0d^7)$, the excited $Fe^+(s^1d^6) + Fe(s^1d^7)$, or the very high-energy $Fe^{+2}(s^0d^6) + Fe^-(s^2d^7)$. Of course, other asymptotes such as the ground-state $Fe(s^2d^6) + Fe^+(s^1d^6)$ occupancy also exist, and are of $\sigma^3d^nd^n$ character. They are not included in the present analysis that focuses on states with two electrons in s-based orbitals.

To extend our earlier analysis to the cases discussed above, the following steps are followed:

1. The d^nd^{n+1} d-orbital configurations are symmetry adapted to form g and u Slater determinant combinations:

$$\psi_g = (2)^{-1/2} [|d^nd^{n+1}| + |d^{n+1}d^n|]$$

$$\psi_u = (2)^{-1/2} [|d^nd^{n+1}| - |d^{n+1}d^n|],$$

where the notation d^nd^{n+1}, for example, indicates that the atom on the left has a d^n configuration and the atom on the right has a d^{n+1} configuration.

2. The six configurations arising from s^2s^0, s^0s^2, and s^1s^1 orbital occupancies (the former two being singlets and the latter producing three degenerate triplets and one singlet) are also combined into g and u Slater determinant symmetry functions:

$$\psi_g^{het} = (2)^{-1/2} [|s^2\ s^0| + |s^0\ s^2|]$$

$$\psi_u^{het} = (2)^{-1/2} [|s^2\ s^0| - |s^0\ s^2|]$$

$$\psi_g^{homo} = (2)^{-1/2} [|s\alpha\ s\beta| - |s\beta\ s\alpha|]$$

(n.b., the two s orbitals refer to the orbitals on the left and right atoms) all of

which are singlet states and contain heterolytic (het) and homolytic (homo) fragments, and

$$\psi_u^{homo} = |s\alpha\ s\alpha|$$

$$\psi_u^{homo} = |s\beta\ s\beta|$$

$$\psi_u^{homo} = (2)^{-1/2}\ [|s\alpha\ s\beta| + |s\beta\ s\alpha|]$$

which are triplets with $M_s = 1$, -1, and 0, respectively.

3. The two d and six s orbital configurations are combined to produce twelve functions whose overall symmetry is g or u. This can be done within the singlet-state manifold as follows:

$$\Psi^{het}_{g,g} = (2)^{-1/2}\ [|s^2\ s^0| + |s^0\ s^2|]\ (2)^{-1/2}\ [|d^n d^{n+1}| + |d^{n+1} d^n|]$$

$$\Psi^{het}_{u,u} = (2)^{-1/2}\ [|s^2\ s^0| - |s^0\ s^2|]\ (2)^{-1/2}\ [|d^n d^{n+1}| - |d^{n+1} d^n|]$$

$$\Psi^{homo}_{g,g} = (2)^{-1/2}\ [|s\alpha\ s\beta| - |s\beta\ s\alpha|]\ (2)^{-1/2}\ [|d^n d^{n+1}| + |d^{n+1} d^n|]$$

all of which are of g symmetry; and

$$\Psi^{het}_{g,u} = (2)^{-1/2}\ [|s^2\ s^0| + |s^0\ s^2|]\ (2)^{-1/2}\ [|d^n d^{n+1}| - |d^{n+1} d^n|]$$

$$\Psi^{het}_{u,g} = (2)^{-1/2}\ [|s^2\ s^0| - |s^0\ s^2|]\ (2)^{-1/2}\ [|d^n d^{n+1}| + |d^{n+1} d^n|]$$

$$\Psi^{homo}_{g,u} = (2)^{-1/2}\ [|s\alpha\ s\beta| - |s\beta\ s\alpha|]\ (2)^{-1/2}\ [|d^n d^{n+1}| - |d^{n+1} d^n|]$$

all of which are of u symmetry. For the triplet states, one can form

$$\Psi^{T,homo}_{u,u} = |s\alpha\ s\alpha|\ (2)^{-1/2}\ [|d^n d^{n+1}| - |d^{n+1} d^n|]$$

(and the corresponding $M_S = -1$ and 0 states) which are of g symmetry, and

$$\Psi^{T,homo}_{u,g} = |s\alpha\ s\alpha|\ (2)^{-1/2}\ [|d^n d^{n+1}| + |d^{n+1} d^n|]$$

(and the corresponding $M_S = -1$ and 0 states) which are of u symmetry.

4. In principle, all of the above configurations of a given g, u and of a given spin symmetry mix to produce the true electronic states of the corresponding symmetries. This mixing can, however, be anticipated by noting that there are two (one g and one u) singlet heterolytic states that contain only $s^2d^n + s^0d^{n+1}$ configurations,

$$(2)^{-1/2}\ [\Psi^{het}_{g,g} + \Psi^{het}_{u,u}] = (2)^{-1/2}\ [s^2d^n\ s^0d^{n+1} + s^0d^{n+1}\ s^2d^n]$$

$$(2)^{-1/2}\ [\Psi^{het}_{g,u} + \Psi^{het}_{u,g}] = (2)^{-1/2}\ [s^2d^n\ s^0d^{n+1} - s^0d^{n+1}\ s^2d^n]$$

as well as two (one g and one u) singlet heterolytic states that contain only $s^0d^n + s^2d^{n+1}$ configurations,

$$(2)^{-1/2}\ [\Psi^{het}_{g,g} - \Psi^{het}_{u,u}] = (2)^{-1/2}\ [s^0d^n\ s^2d^{n+1} + s^2d^{n+1}\ s^0d^n]$$

$$(2)^{-1/2}\ [\Psi^{het}_{g,u} - \Psi^{het}_{u,g}] = (2)^{-1/2}\ [s^0d^n\ s^2d^{n+1} - s^2d^{n+1}\ s^0d^n].$$

Configurations of the form $s^1d^n + s^1d^{n+1}$ are represented by a total of eight homolytic states; two singlets

$$\Psi^{homo}_{g,g} = (2)^{-1/2}\ [|s\alpha\ s\beta| - |s\beta\ s\alpha|]\ (2)^{-1/2}\ [|d^nd^{n+1}| + |d^{n+1}d^n|]$$

$$\Psi^{homo}_{g,u} = (2)^{-1/2}\ [|s\alpha\ s\beta| - |s\beta\ s\alpha|]\ (2)^{-1/2}\ [|d^nd^{n+1}| - |d^{n+1}d^n|]$$

and two triplets ($M_S = 1$)

$$\Psi^{T,homo}_{u,u} = |s\alpha\ s\alpha|\ (2)^{-1/2}\ [|d^nd^{n+1}| - |d^{n+1}d^n|]$$

$$\Psi^{T,homo}_{u,g} = |s\alpha\ s\alpha|\ (2)^{-1/2}\ [|d^nd^{n+1}| + |d^{n+1}d^n|]$$

with their corresponding $M_S = -1$ and 0 functions.

Correlations for a species such as the Fe_2^+ ion discussed in the text, in which the $s^2d^n + s^0d^{n+1}$ asymptote lies lowest, the $s^1d^n + s^1d^{n+1}$ next, and $s^0d^n + s^2d^{n+1}$ highest, are: 1) the two (one g and one u) $s^2d^n + s^0d^{n+1}$ asymptotes correlate to the two (one g and one u) $\sigma_g^2d^nd^{n+1}$ bonding molecular states; 2) the two (one g and one u) high-energy $s^0d^n + s^2d^{n+1}$ asymptotes correlate to the two (one g and one u) $\sigma_u^{*2}d^nd^{n+1}$ antibonding molecular states; and 3) the eight (one singlet g, three triplet g, one singlet u, and three triplet u) $s^1d^n + s^1d^{n+1}$ asymptotes correlate to the eight $\sigma_g^1\sigma_u^{*1}d^nd^{n+1}$ antibonding molecular states. Hence, one set (g and u) of attractive curves connecting to the low-energy heterolytic fragments, four sets (g and u) of repulsive curves connecting to the homolytic fragments, and one set (g and u) of repulsive curves connecting to the high-energy heterolytic fragments are expected in such

cases. Such potential curves are illustrated in Fig. 4. In effect, if the d^n core is viewed as X and the d^{n+1} core as Y, the results derived here are equivalent to those of Appendix A for heteronuclear systems, Figs. 3 - 5.

Acknowledgment. J. S.'s efforts were supported in part by the Office of Naval Research and by NSF Grants #CHE8814765 and #CHE9116286. P. B. A.'s research is supported by the Division of Chemical Sciences, Office of Basic Energy Sciences, U. S. Department of Energy and by NSF Grant #CHE8917980. We would also like to thank Profs. Chuck Wight and Michael Morse for useful discussion.

References

1. Shaik, S., J. Org. Chem. **1983**, 52, 1563.
2. Shaik, S., J. Am. Chem. Soc. **1981**, 103, 3692.
3. Poss, A.; Shaik, S., J. Am. Chem. Soc. **1981**, 103, 3702.
4. Poss, A.; Shaik, S., J. Am. Chem. Soc. **1982**, 104, 187.
5. Poss, A.; Shaik, S., Acc. Chem. Res. **1983**, 16, 363.
6. Michl, J. Acc. Chem. Res. **1990**, 23, 127.
7. Dearden, D. V.; Hayashibara, K.; Beauchamp, J. L.; Kirchner, N. J.; van Koppen, P. A. M.; Bowers, M. T., J. Am. Chem. Soc. **1989**, 111, 2401.
8. Schultz, R. H.; Crellin, K. C.; Armentrout. P. B. J. Am. Chem. Soc. **1991**, 113, 8590.
9. Willey, K. F.; Cheng, P. Y.; Pearce, K. D.; Duncan, M. A. J. Phys. Chem. **1990**, 94, 4769.

10. Lias, S. G.; Bartmess, J. E.; Liebman, J. F.; Holmes, J. L.; Levin, R. D. ; Mallard, W. G. J. Phys. Chem. Ref. Data 1988, 17, Suppl 1.

11. Willey, K. F.; Cheng, P. Y.; Bishop, M. B.; Duncan, M. A. J. Am. Chem. Soc. 1991, 113, 4721.

12. Loh, S. K.; Lian, L.; Hales, D. A.; Armentrout, P. B. J. Phys. Chem. 1988, 92, 4009.

13. Hales, D. A. ; Armentrout, P. B., J. Cluster Sci. 1990, 1, 127.

14. Lian, L.; Su, C-X; Armentrout, P. B. Chem. Phys. Lett. 1991, 180, 168.

15. Morse, M. D. Chem. Rev. 1986, 86, 1049.

16. Rohlfing, E. A.; Cox, D. M.; Kaldor, A.; Johnson, K. H. J. Chem. Phys. 1984, 81, 3846.

17. Energies for the electronic states are cited as the difference between the lowest energy J levels and taken from Sugar, J.; Corliss, C. J. Chem. Phys. Ref. Data 1985, 14, Suppl. 2.

18. Lessen, D.; Brucat, P. J., Chem. Phys. Lett. 1988, 149, 473.

19. Bauschlicher, C. W.; Partridge, H.; Langhoff, S. R. submitted for publication.

20. Upton, T. H.; Goddard, W. A., J. Am. Chem. Soc. 1978, 100, 5659.

21. Indeed, as pointed out to us by Prof. M. D. Morse, states with different couplings of the d orbital configurations will also lead to families of attractive and repulsive curves. For example, Co^+ in its ^3F, ^1G, ^1D, ^3P, or ^1S states (all having an s^0d^8 configuration) will interact with $Ni(^3F,s^2d^8)$ along attractive potential curves. Repulsive curves will evolve from the corresponding $Co(s^1d^8)$ + $Ni^+(s^1d^8)$ and $Co^-(s^2d^8)$ +

$Ni^{+2}(s^0d^8)$ asymptotes. Similar considerations also hold for homonuclear transition metal systems.

22. Simons, J. Energetic Principles of Chemical Reactions, Jones and Bartlett, Boston, Mass. (1983).

FIGURE CAPTIONS

Figure 1. State correlation diagram for dissociation of a homonuclear species in which homolytic bond cleavage is energetically favored. Singlet surfaces are shown by solid lines and triplets by dashed lines.

Figure 2. State correlation diagram for dissociation of a homonuclear species in which heterolytic bond cleavage is energetically favored. Singlet surfaces are shown by solid lines and triplets by dashed lines.

Figure 3. State correlation diagram for dissociation of a heteronuclear species in which homolytic bond cleavage is energetically favored. Singlet surfaces are shown by solid lines and triplets by dashed lines.

Figure 4. State correlation diagram for dissociation of a heteronuclear species in which heterolytic bond cleavage to one product is energetically favored but homolytic cleavage lies below the second heterolytic asymptote. Singlet surfaces are shown by solid lines and triplets by dashed lines.

Figure 5. State correlation diagram for dissociation of a heteronuclear species in which both heterolytic bond cleavage products are energetically favored relative to homolytic cleavage. Singlet surfaces are shown by solid lines and triplets by dashed lines.

Figure 6. Schematic potential energy surfaces depicting the interaction of CO with $Mn(CO)_x^+$ in its ground and first excited electronic state. Reproduced from reference 7 with permission of the American Chemical Society.

Figure 7. Schematic potential energy surfaces for $(AgC_6H_6)^+$. Reproduced from reference 11 with permission of the American Chemical Society.

Figure 8. Qualitative potential energy surfaces for Ni_2^+ including molecular states with one (dotted lines), two (solid lines) and three (dashed lines) σ electrons. Note that the surfaces for states with 2 σ electrons correspond to those shown in Fig. 4.

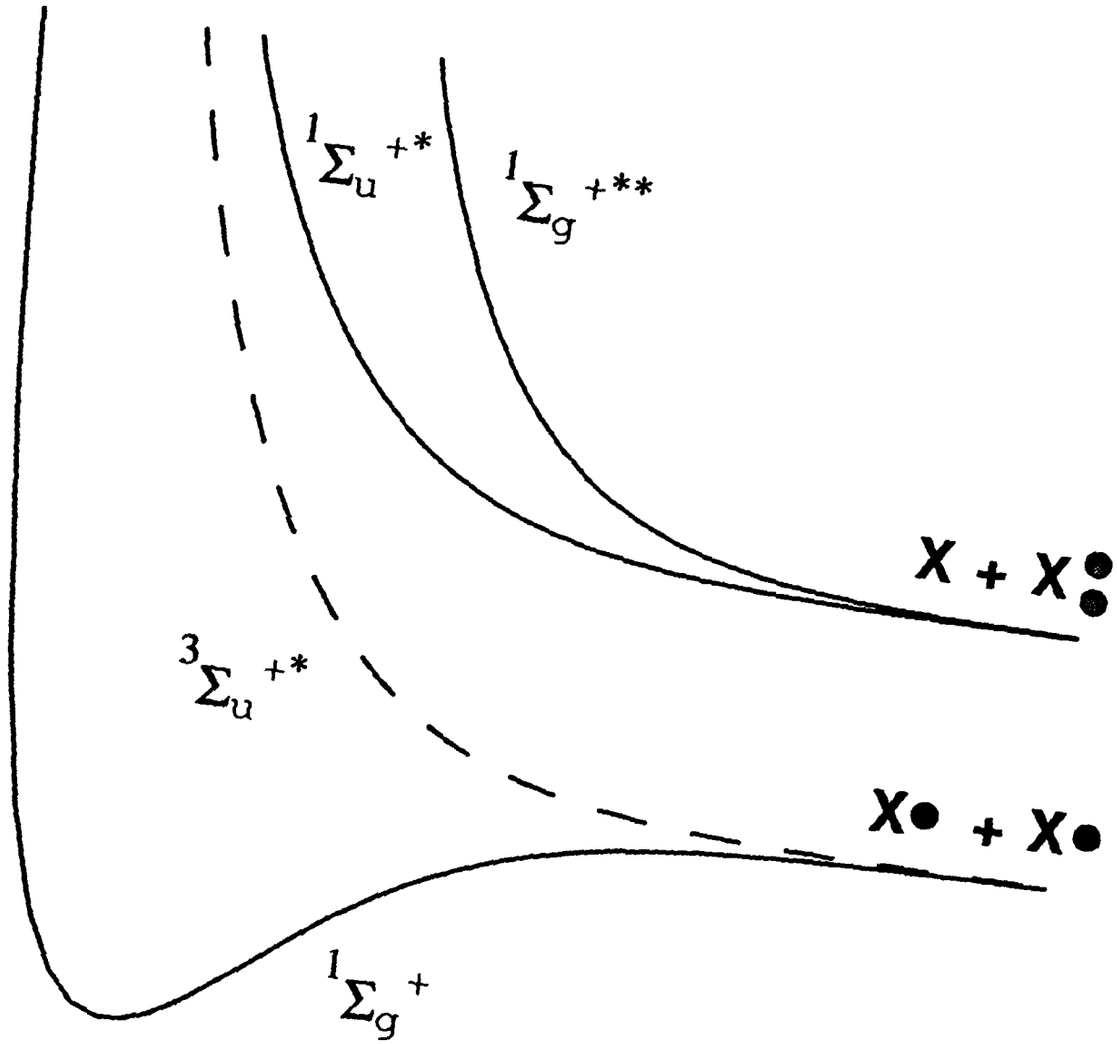

Figure 1

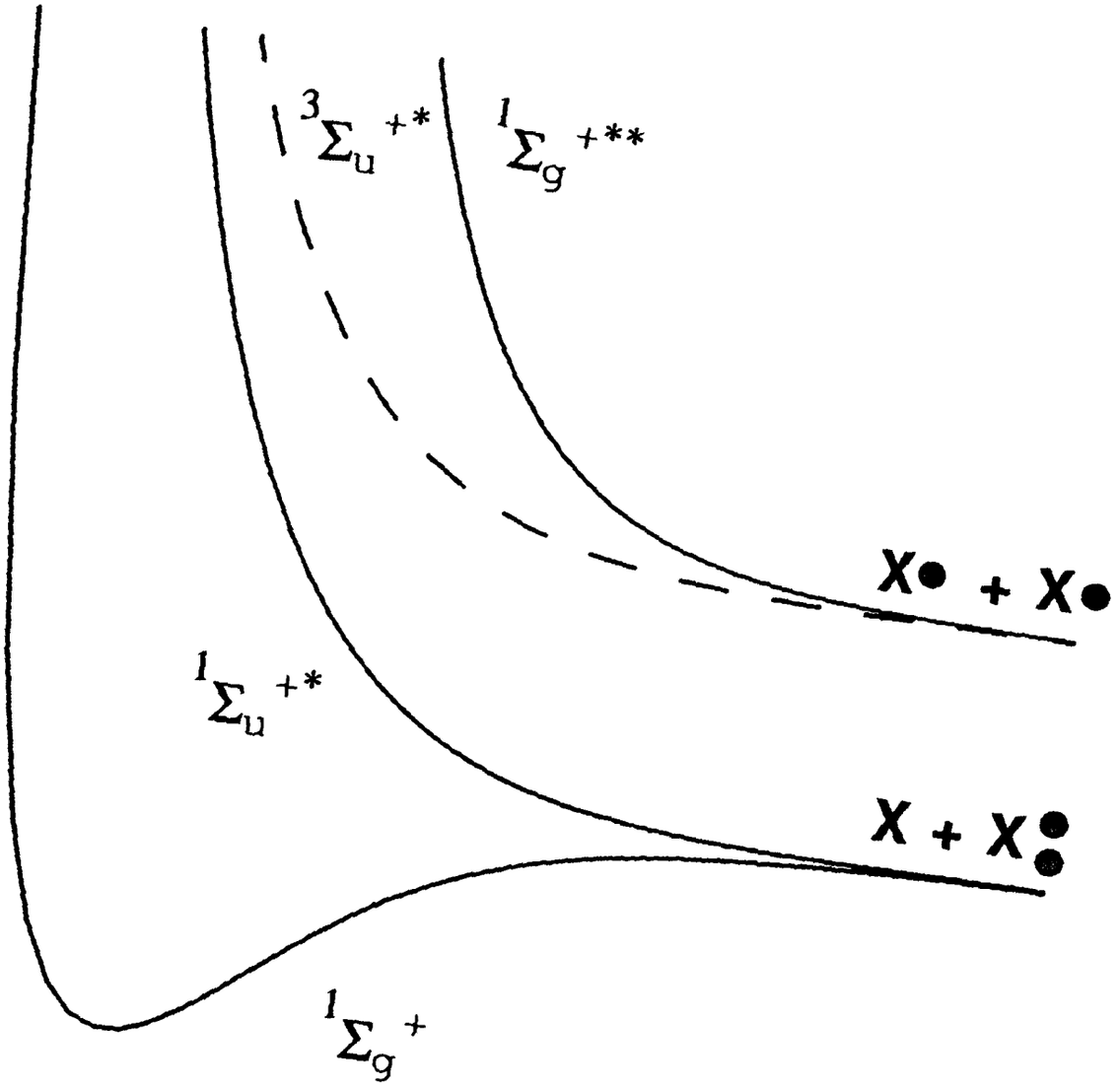

Figure 2

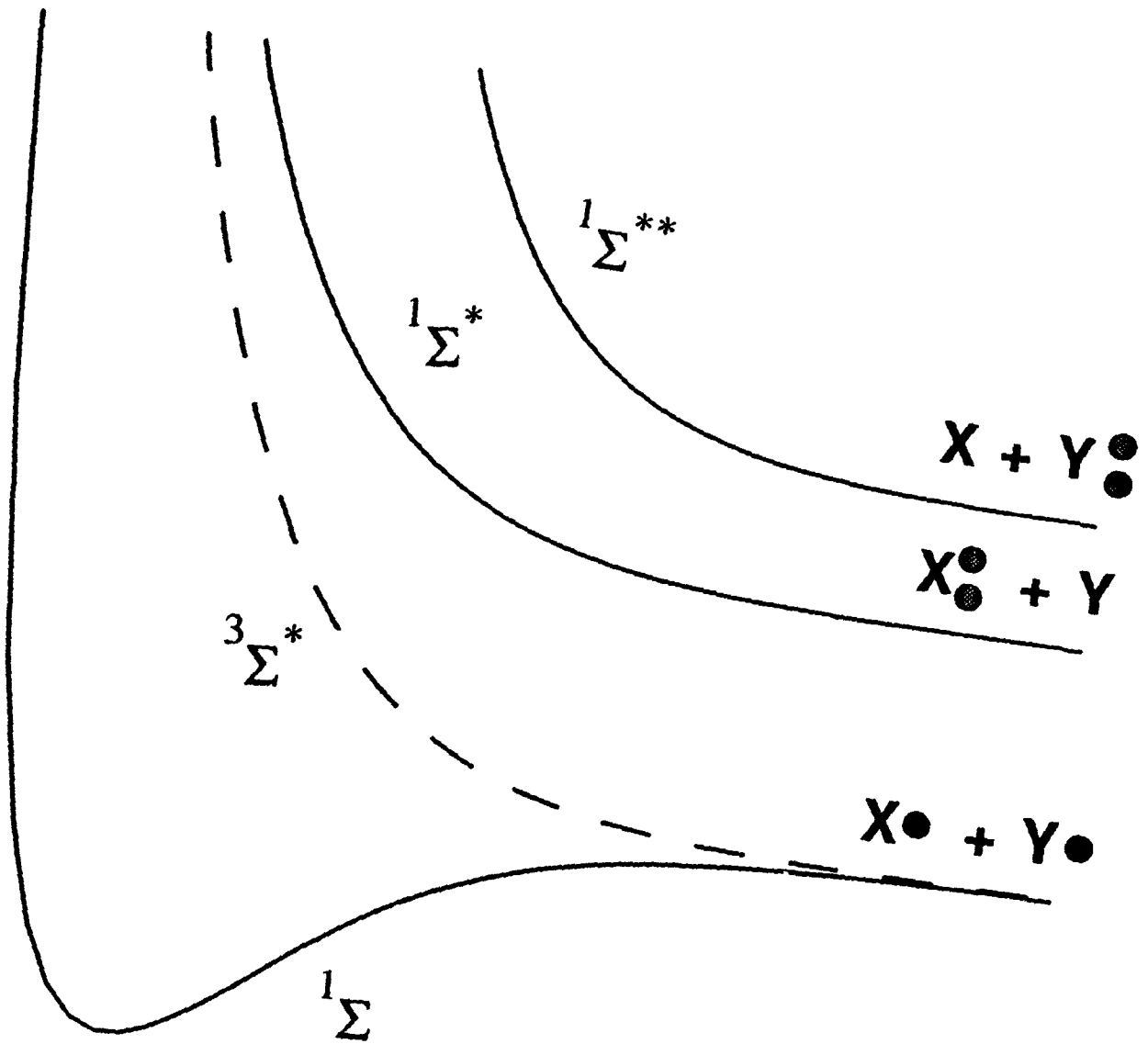

Figure 3

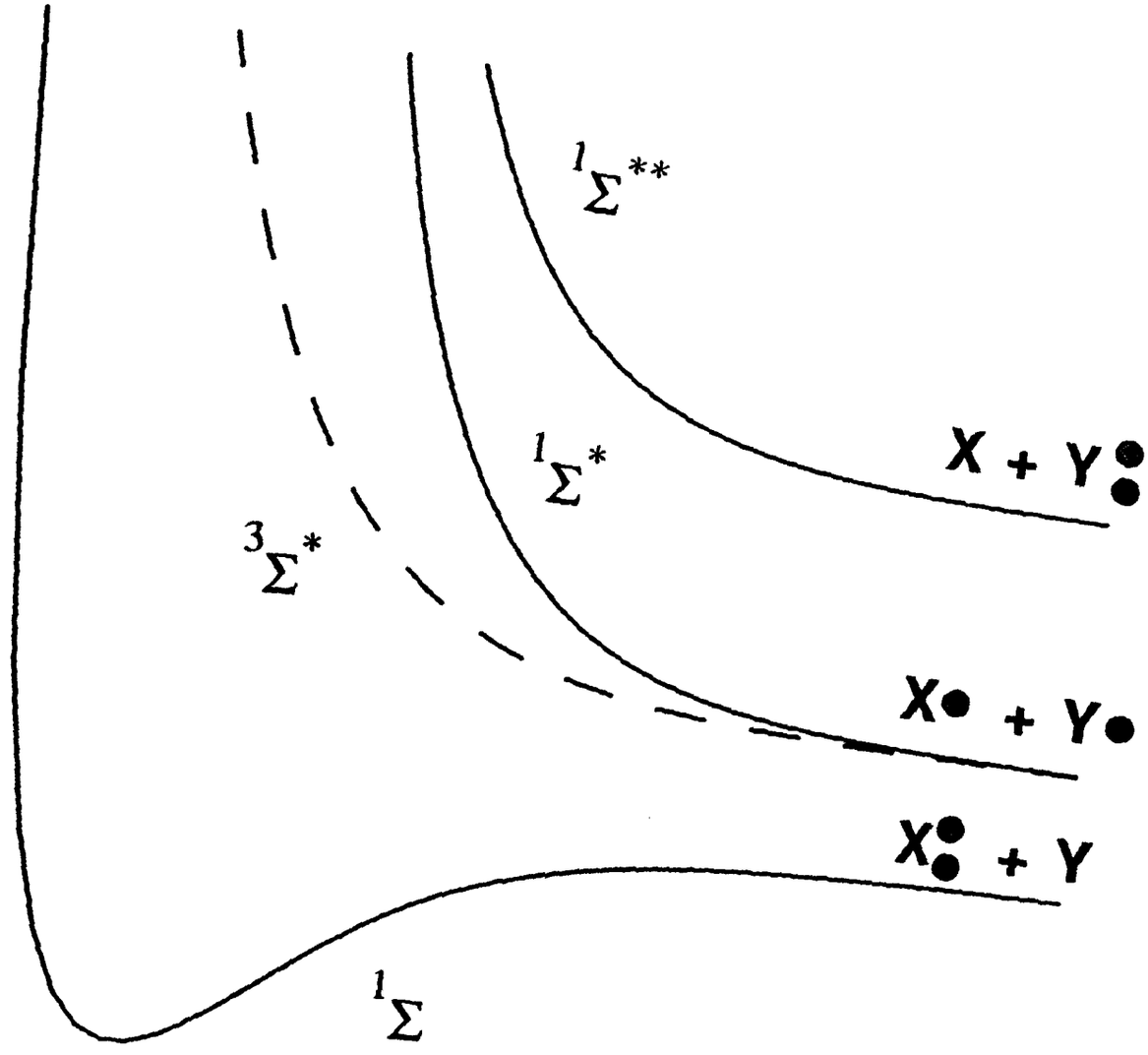

Figure 4

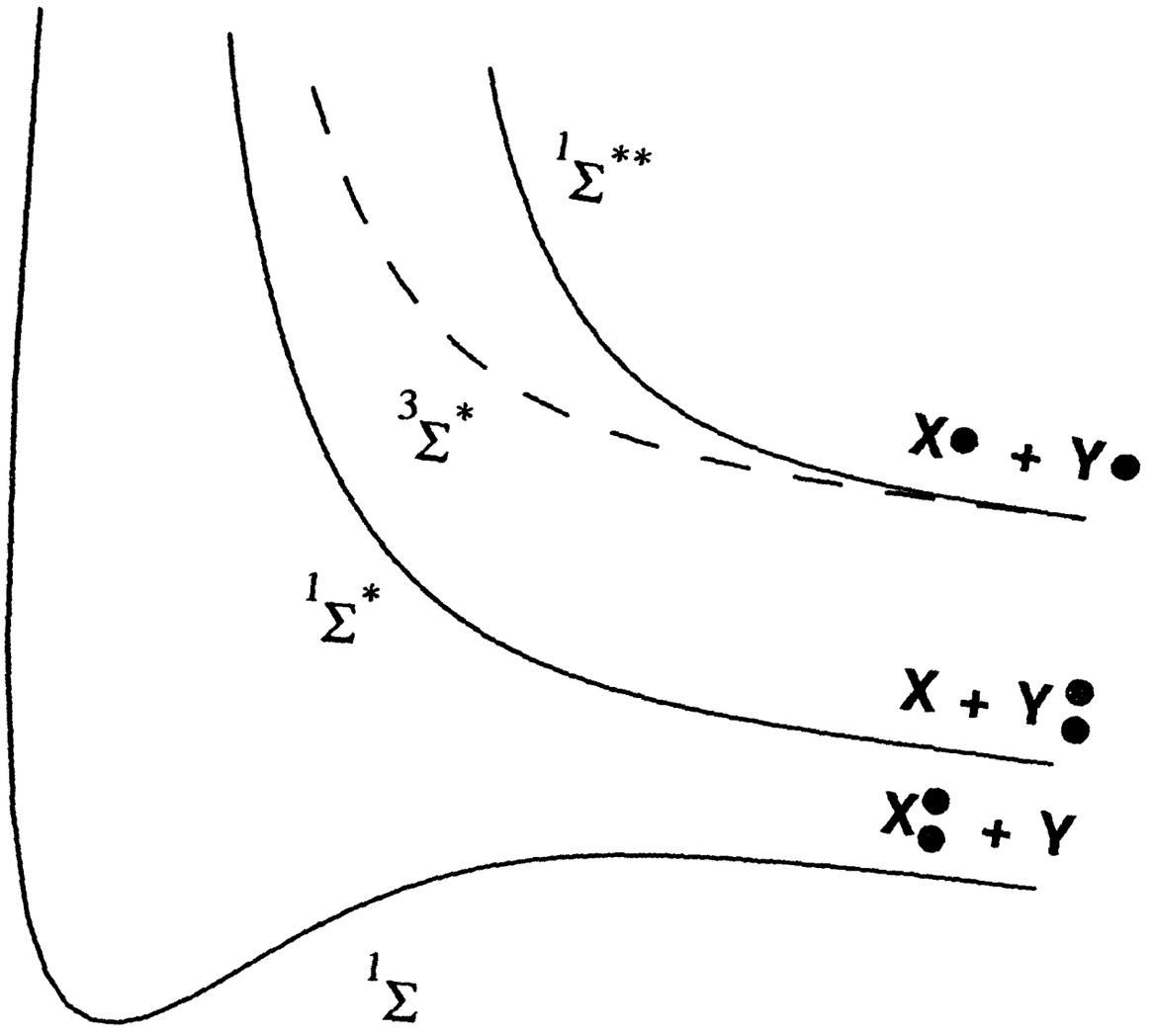

Figure 5

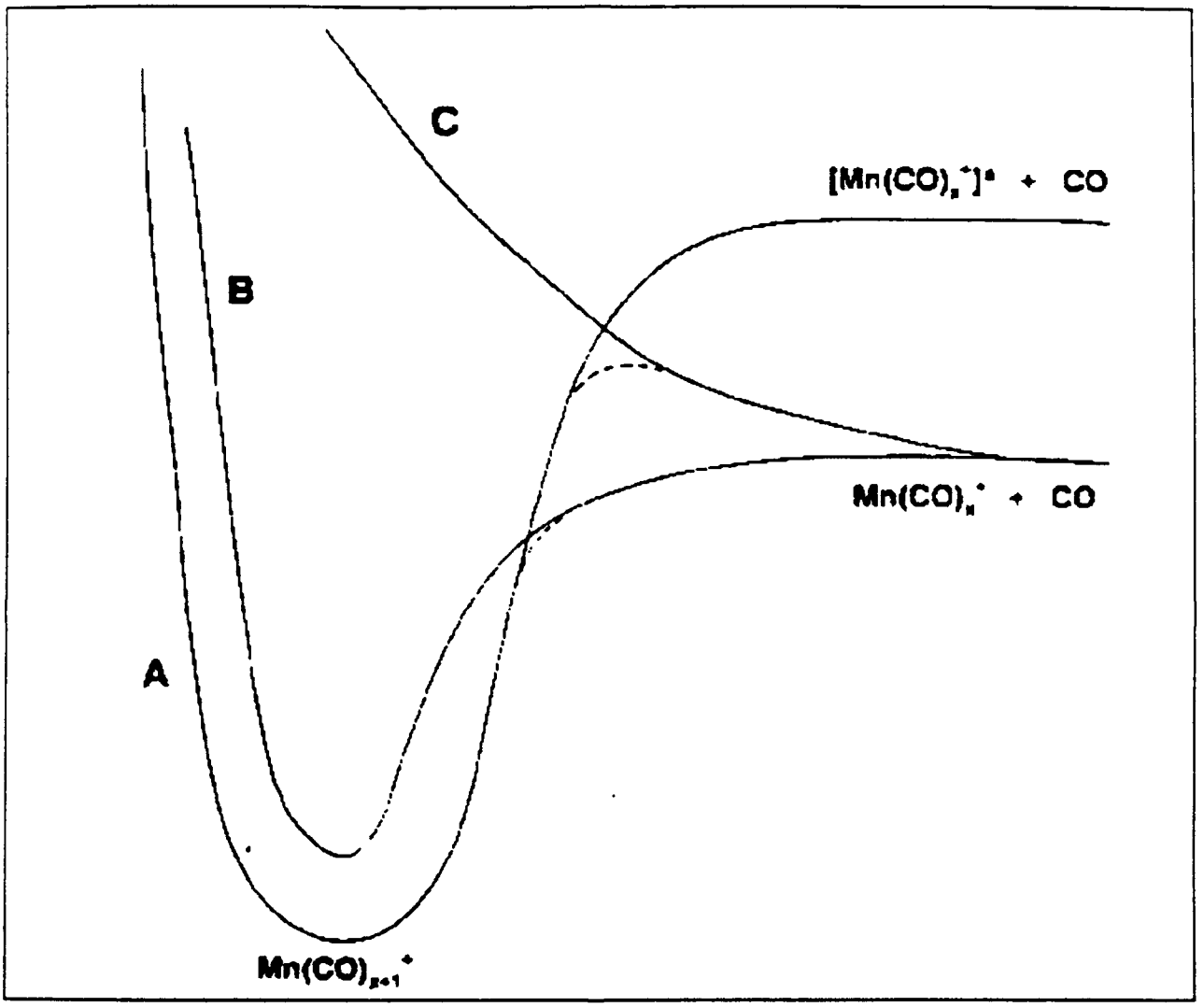

Figure 6

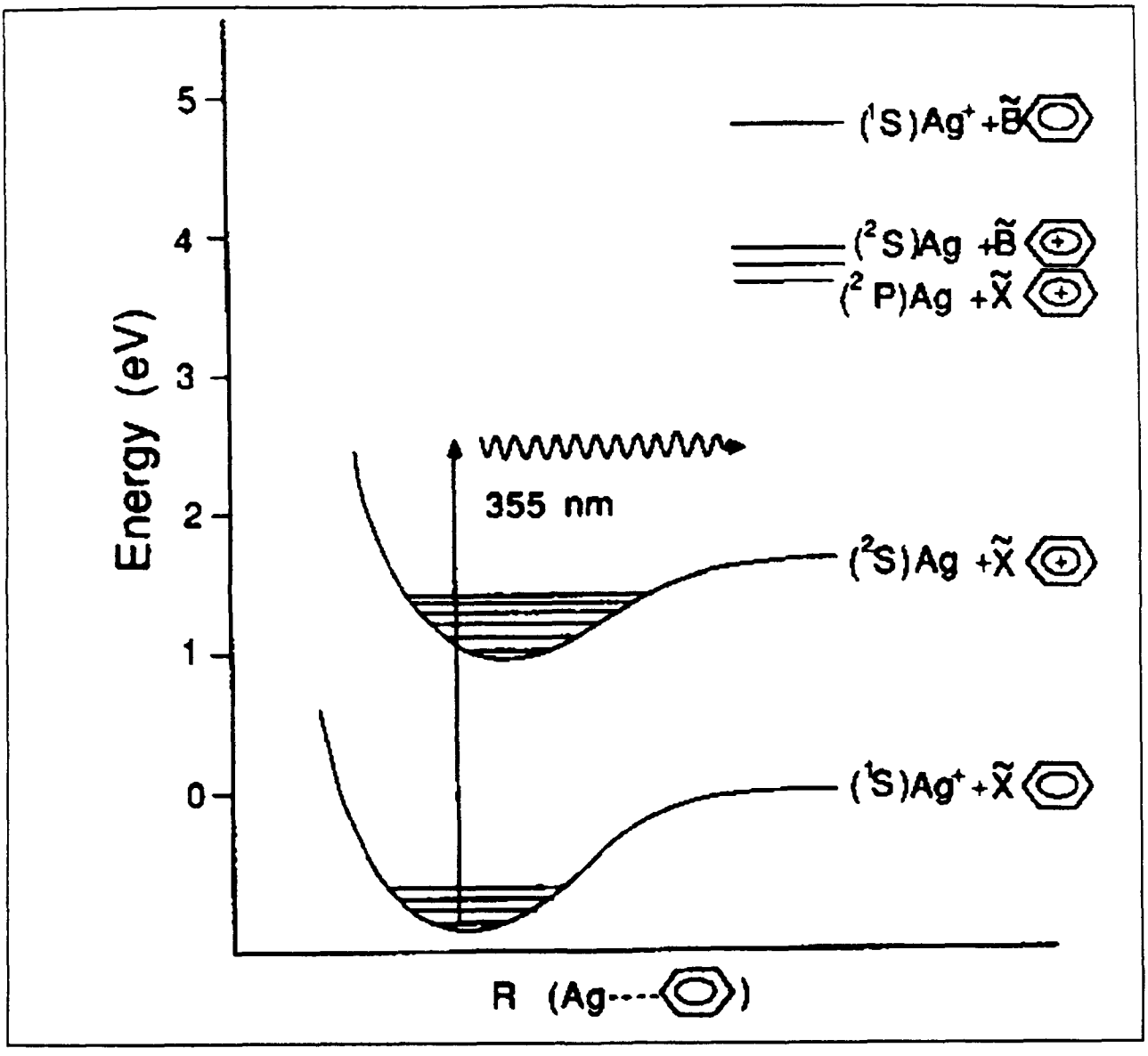
Energy (eV)
5
4
3
2
1
0
(^{1}S)Ag$^+$ +$\tilde{B}$
(^{2}S)Ag +$\tilde{B}$
(^{2}P)Ag +$\tilde{X}$
355 nm
(^{2}S)Ag +$\tilde{X}$
(^{1}S)Ag$^+$ +$\tilde{X}$
R (Ag----)

Figure 7

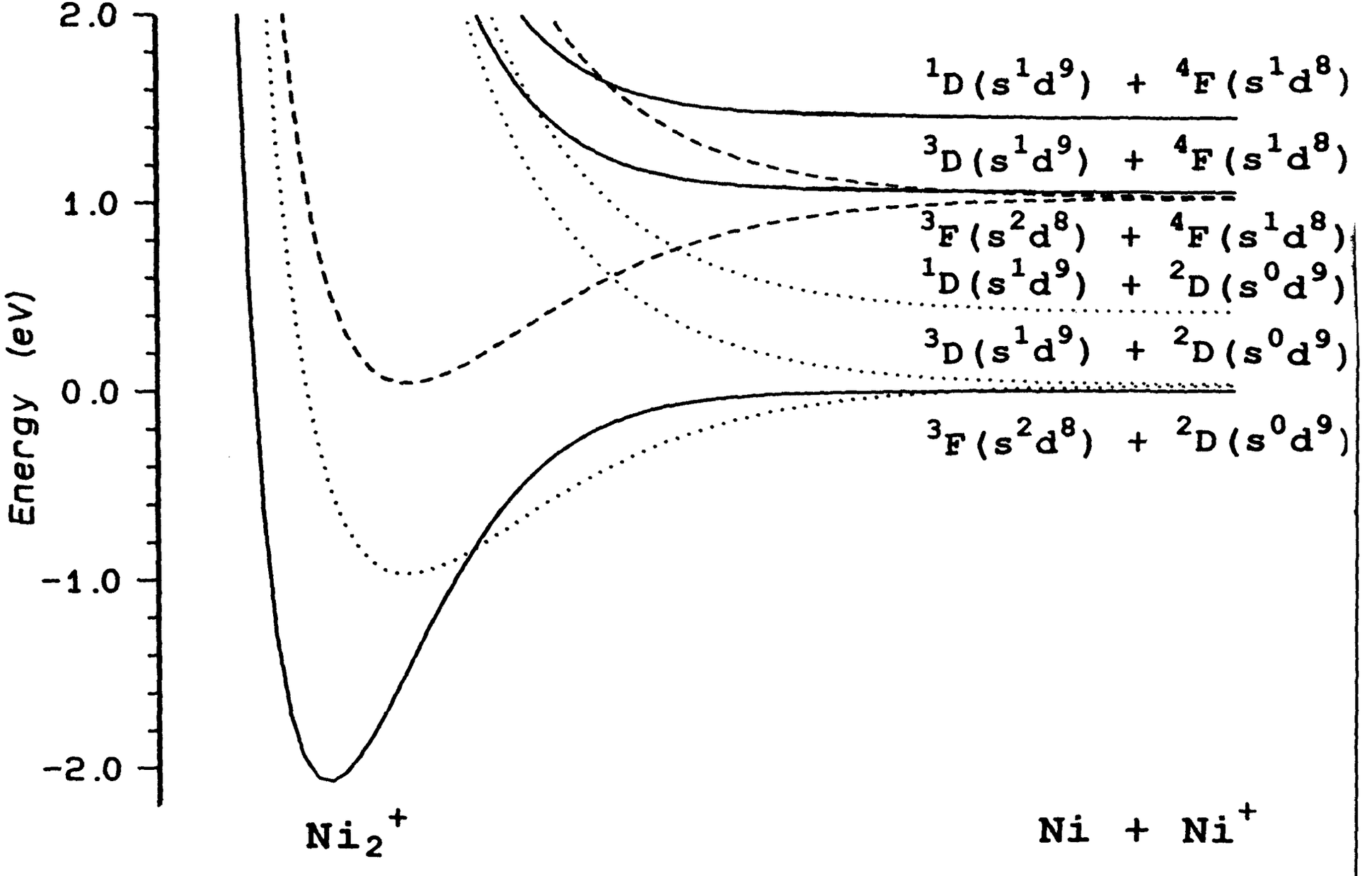
2.0
1.0
0.0
-1.0
-2.0
Energy (eV)
$^1D(s^1d^9) + {}^4F(s^1d^8)$
$^3D(s^1d^9) + {}^4F(s^1d^8)$
$^3F(s^2d^8) + {}^4F(s^1d^8)$
$^1D(s^1d^9) + {}^2D(s^0d^9)$
$^3D(s^1d^9) + {}^2D(s^0d^9)$
$^3F(s^2d^8) + {}^2D(s^0d^9)$
Ni_2^+
$Ni + Ni^+$

Figure 8